Aerodynamic Metrologists Guide to Dynamic Force Measurement

Devin E. Burns*
NASA Langley Research Center, Hampton, Virginia 23681
Nicholas Vlajic†
The Pennsylvania State University Applied Research Laboratory, University Park, Pennsylvania 16802
Ako Chijioke‡
National Institute of Standards and Technology, Gaithersburg, Maryland 20899
and
Peter A. Parker§
NASA Langley Research Center, Hampton, Virginia 23681

https://doi.org/10.2514/1.C036676

Static aerodynamic force measurement is generally of interest in both low- and high-speed ground test facilities, but dynamic force measurement is typically associated with higher-speed facilities. This work will show that dynamic force measurement is relevant to all aerodynamic metrologists because wind tunnel system dynamics can change the force transducer's dynamic sensitivity resulting in differences between the static and dynamic sensitivity. In addition, the field of dynamic force measurement will be introduced using realistic wind tunnel scenarios, wherein the wind tunnel system dynamics contribute to increased uncertainty in what would otherwise be considered a static force measurement. A design approach focused on estimating the dynamic response is presented to achieve measurement objectives through the use of static force measurement techniques where possible. To that end, a reduced-order model is developed to characterize the dynamic response of the system, which can serve as a predictive tool in the design process. Then, strategies for characterizing wind tunnel system dynamics to determine acceptable bandwidths wherein the static measurements may be sufficient are discussed. In the event that systems have undesirable dynamic characteristics, which cannot be avoided in the design process, two dynamic compensation techniques to correct the measured signals are discussed.

I. Introduction

FORCE transducers are commonly calibrated statically but may be used to make time-varying dynamic force measurements. For wind tunnel model systems that incorporate force transducers, the structural dynamics of the test article and supporting structure will result in differences between the force transducer's dynamic and static sensitivities. Dynamic loading may be present in a test intentionally, for example, in aeroelastic studies, or may be present inadvertently, for example, due to turbulence in a nominally steady flow. Under dynamic conditions such as these, the dynamic sensitivity of the force transducer can deviate by several orders of magnitude from the static sensitivity for certain rates (frequencies) of loading [1–3], and lead to unacceptably large errors in the measured response. For some wind tunnel model support systems, differences between the force transducer's static and dynamic sensitivities can be large even in the 1–10 Hz regime.

Within aerodynamic ground testing, wind tunnel model support system dynamics are relevant to many tests. For instance, some tests employ long stings to avoid support system interference on the data, but these long stings frequently result in excessive dynamics [4–6]. In hypersonic facilities, the wind tunnel model support system resonances must be outside a frequency range equivalent to the flow duration; otherwise, unacceptably large errors in the measurement of aerodynamic forces may result [7–11]. For aeroelastic testing, low-frequency resonant modes due to the model support system (usually the sting) can lead to undesirable dynamics particularly if they generate an aeroelastic instability. It is thus common practice to include the wind tunnel model support hardware in finite-element-based modal analyses of the aeroelastic system [12–16].

This work provides an introduction to the field of dynamic force metrology exemplified with applications related to aerodynamic ground test facilities. To better understand the limitations of a force transducer's static sensitivity based on the wind tunnel model support that is used, a reduced-order (lumped parameter two-degree-of-freedom) model is developed. This is a technique commonly used to estimate the primary resonant modes of wind tunnel model support systems [7,17], but will be used here to understand the implications for the force transducer. To support the development of the two-degree-of-freedom model, a finite element analysis method to estimate the translational stiffness of the model support hardware is shown.

The paper prioritizes designing the wind tunnel model system to allow for static force measurement where possible, but also discusses techniques for measuring the dynamic response of the system and dynamic calibration strategies for situations that require measurement bandwidths beyond the region wherein the static calibration gives sufficient accuracy. The example case studies presented here will focus on ground tests that have configurations comprised of a model support system consisting of a wind tunnel balance and sting.

II. Motivating Example

A schematic of a wind tunnel test setup is shown in Fig. 1a, while a simplified reduced-order dynamic model of the physical configuration is shown in Fig. 1b. For illustrative purposes, it is assumed that motion occurs in only one direction, the test article and sting are rigid masses, and the balance has a known stiffness. The dynamic sensitivity of a system such as this is shown in Fig. 2. We note that this is an example response for the parameters chosen and is not a ubiquitous representation for all wind tunnel experiments.

Received 13 September 2021; revision received 10 January 2022; accepted for publication 25 May 2022; published online 14 June 2022.

*Engineer, Advanced Measurement and Data Systems Branch. Member AIAA.
†Assistant Research Professor, Acoustics Department.
‡Physicist, Mass and Force Group, Quantum Measurement Division, Physical Measurement Laboratory.
§Team Lead, Advanced Measurement and Data Systems Branch. Member AIAA.

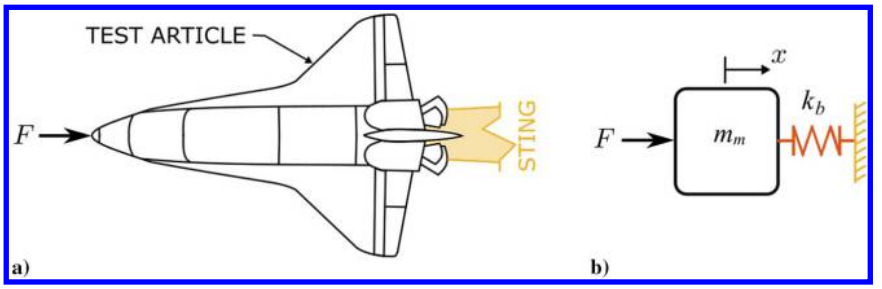

Fig. 1 a) Schematic of a wind tunnel test article mounted onto a balance on a rigid sting. b) An equivalent reduced-order dynamic model of the system.

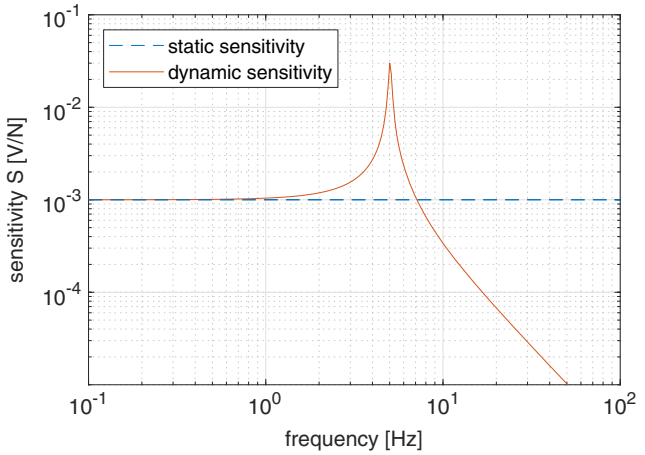

Fig. 2 Representative dynamic sensitivity of an example force balance compared to the static sensitivity (assumed to be constant over the bandwidth).

The errors that may arise when using the static sensitivity to make measurements of time varying signals are demonstrated by simulating a system that has the sensitivity shown in Fig. 2 subjected to a force with both static (DC) and dynamic (AC) characteristics. These forces may be representative of the integrated forces acting on a test article in wind tunnel testing. For this force profile, the static component aims to capture the forces originating from constant aerodynamic loading, while the dynamic component may represent forces generated by turbulence or unsteady lift forces in the flowfield. Force 1, shown in Fig. 3a, has a static component of 1000 N and a dynamic component characterized by a root-mean-square (RMS) amplitude of 5.86 N. The dynamic portion of the signal has low-frequency oscillations as can be seen in the time domain of Fig. 3a, and in the frequency domain representation provided in Fig. 3g. Note that the static component of the force, namely, the 1000 N, would be apparent in the 0 Hz bin (or DC bin) of the frequency domain plot, but 0 Hz is not shown on the log scale. The indicated force, determined by converting the output of the force transducer to units of force using the static sensitivity, is shown in the time domain signal of Fig. 3b and in the frequency domain of Fig. 3h. Although the differences between

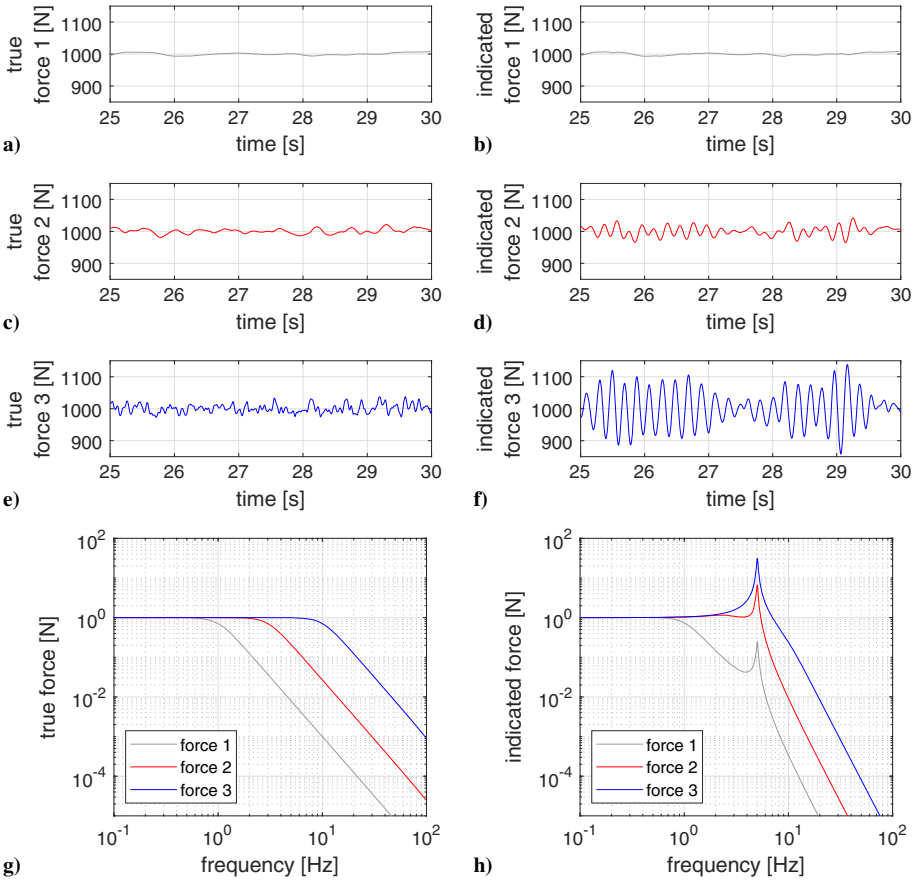

Fig. 3 Time domain representations of true applied a) force 1, c) force 2, and e) force 3 and the measured forces using a constant sensitivity (b, d, f). g) Applied forces 1–3 shown in the frequency domain. h) Measured forces 1–3 shown in the frequency domain.

the time domain input and output are almost indiscernible on this scale, the RMS of the signal is 7.74 N, which corresponds to a relative error of 32% for the dynamic portion of the force. The presence of this error is apparent in the frequency domain representation shown in Fig. 3h, wherein there is a small amplitude around the mechanical resonance of the system. It is noted that the mean of the output, representing the static portion, correctly indicates 1000 N.

As the bandwidth of the applied force increases beyond 1 Hz, the static and dynamic sensitivity start to deviate (Fig. 2), implying a larger error for faster forces. Force 2, shown in Fig. 3c, has faster frequency oscillations than Force 1, and Fig. 3g shows that this force has appreciable energy content in the region where the dynamic calibration starts to have appreciable deviations from the static sensitivity, namely, the 3–5 Hz regime. The small-amplitude, high-frequency oscillations in Force 2, are amplified by the system dynamics and are visible in Fig. 3d. This amplification is apparent in Fig. 3h near the resonant regime. Here, the time domain relative RMS amplitude error is 91.6%, but the mean is still 1000 N.

As the rate of the applied force is increased even further, such as Force 3 in Fig. 3e, there is significant energy within the bandwidth regime that contains the resonance of the system (Fig. 3g). As can be seen in the time history of Figs. 3f and 3h, the dynamic portion of the signal is amplified by the mechanical resonance of the system. Here, the dynamic errors become large and a static sensitivity is likely not sufficient for many applications. Although the dynamic portion of the signal has a relative RMS amplitude error of 299.5%, the static portion of the indicated force still yields 1000 N.

Note that, in all three cases, the mean of the output force of the balance is approximately 1000 N, which is equivalent to the static component of the true force. Only the time-dependent portion of the balance signal will cause errors in the determination of the true force application to the system.

III.

Within this section, strategies are presented to aid wind tunnel aerodynamicists in improving dynamic force measurements. The design strategies are effectively drawn from structural dynamics and modal testing practices that involve modeling and verification through measurement [18,19]. The dynamic compensation methods have been adapted from the dynamic metrology literature.

1) *Design for dynamic measurements:* Considerations for dynamic measurements are intended to occur early in the test design process. Within this stage, the structural dynamics and natural frequencies of the test configuration are estimated for the desired test article and candidate force balances and stings. The dynamics are predicted using either finite element analysis (FEA) or reduced-order modeling. At this stage, reduced-order modeling is attractive because the dynamics can be estimated quickly given the physical properties (e.g., inertia and stiffness) of the candidate wind tunnel model parts. In Sec. III.A.1, we present a reduced-order structural dynamics model, which represents typical wind tunnel test article and sting assemblies and can be used to a priori estimate the usable bandwidth wherein a static sensitivity may be used without significant errors. By aid of FEA or reduced-order modeling, design changes may be made to achieve the desired structural response.

2) *Measurement of the dynamic response:* Once the test article, balance, and sting have been selected and installed in the desired test configuration, the dynamic response can be measured to validate the predicted dynamics and determine the bandwidth that static sensitivity may be used to make dynamic measurements. Here, the test configuration is excited using either an applied force or given initial condition (e.g., pulling/pushing on the model and quickly releasing) and recording the response of the balance. Performing a Fourier transform of the time series or examining the response on a spectrum analyzer will yield information on the resonances and antiresonances of the system. The applied force or initial conditions do not necessarily need to be known or measured to determine the resonances.

3) *Dynamic compensation:* We present two dynamic compensation strategies, namely, an acceleration compensation method and a dynamic calibration. The acceleration compensation combines an additional acceleration measurement along with a reduced-order model to make an inertial correction of the measured force. In principle, if the measured dynamic response was obtained using a known calibrated force and the responses of the balance are recorded, then the information needed for a dynamic calibration has already been obtained. To use this dynamic calibration, a deconvolution or inversion of the system response must be determined. This process is briefly reviewed, but we note that this process presents mathematical and numerical challenges that are beyond the scope of this paper.

These approaches are not mutually exclusive. In fact, designing the measurement system with dynamic requirements in mind should be prioritized as it can limit the need for dynamic compensation. Nevertheless, it is beneficial to have a broader appreciation for when it may be appropriate to implement some of these techniques and what the potential ramifications of doing so are. Thus, Table 1 summarizes pros and cons associated with the implementation of these techniques.

A. Design for Dynamic Measurements

In the experimental design process, the shape and scale of an aerodynamic model are selected, then a specific force balance and sting are chosen based on the anticipated force ranges. If specific information is available on the dynamic forces generated by the wind tunnel flow for the model of interest, then this information should also be considered as the balance and model support hardware are chosen. Once these parts have been identified, a finite element model or reduced-order model of the test configuration including the test article, force balance, sting, and supporting structure of the sting may be used to estimate the bandwidth wherein the static calibration is valid.

If the usable bandwidth of the static calibration is not sufficient for the test objectives, design considerations should first be considered to determine if the usable bandwidth of the static calibration can be expanded. A few physical changes that can be considered include the following:

1) The mass of the test article can be reduced to increase the first natural frequency of interest. Potential avenues to reduce mass include reducing the test article size, constructing the test article by additive manufacturing with lightweighting considerations, or selecting a different material.

2) A stiffer force balance can be selected or designed.

3) The sting can be made stiffer and lighter.

4) Damping can be used to reduce resonant oscillation at the natural frequencies to an acceptable level or to a level where further measurement is possible, although in practice it is often challenging to physically implement the desired damping level.

There is historical precedent for these types of changes within wind tunnel testing. Balances employing semiconductor and piezoelectric strain measuring elements have been used in hypersonic facilities [9,17,20,21] to allow the balance to be stiffened while still maintaining sufficient measurement resolution. Reducing test article mass (size) is also mentioned as a design consideration [9], but it needs to be done with aerodynamic measurement objectives in mind. Similarly, the importance of sting design has been highlighted for blunt body dynamic stability testing within supersonic flows [22]. Finally, both active [4] and passive damping [6] have been used to help control the response of wind tunnel model support systems.

An additional important design consideration is hardware filtering in the data acquisition. If static loads are being measured, hardware or software filtering can be used to remove dynamic content from the acquired signal. The use of predigitization hardware filtering has the advantage of maximizing available digitizer dynamic range, which in many cases results in data with a higher signal-to-noise ratio. In the case where dynamic loads are to be measured and where the mechanical design is not able to sufficiently expand the static bandwidth, hardware filtering can be advantageous in suppressing resonant

Table 1 High-level comparison of the approaches discussed in the text for handling balance dynamic measurements

Method	Pros	Cons	Comment
Design for dynamic measurements	• Can eliminate the need for taking further measures • Will generally increase the measurable bandwidth even if further measures are still needed	• In some cases it will not be possible to eliminate the need for additional measures.	This should always be the first step in dealing with possible dynamic loading, whether such loading is intentional or otherwise.
Measurement of dynamic response	• Will show for the physically realized test assembly whether the dynamic response is likely to affect measurement results • Can be a simpler procedure than engaging in a calibration and compensation	• Tests can increase the cost and schedule of time in the tunnel facility.	A prerequisite for a compensation based on dynamic calibration
Acceleration compensation	• Can be a relatively mathematically straightforward way to correct most of the dynamic error in the balance output • Accurate acceleration measurement to high bandwidth (several kilohertz) is available using off-the-shelf equipment	• Accuracy and applicable bandwidth depend on the validity of the model used; for some measurements the simplest models may not be adequate. • Limited by the accuracy of the acceleration measurements • Increase in the number of sensors	The acceleration response can be measured in situ without the need for a dynamic model [27,28], but we classify this as a dynamic calibration.
Dynamic calibration	• Not reliant on modeling approximations beyond linearity and time-invariance • All system response terms to the externally applied force are intrinsically accounted for.	• Somewhat involved mathematical requirements for applying dynamic correction to many measurements, including the need to stabilize against noise. • In some cases it is difficult to apply a calibration force with a spatial profile similar to the test force. • Uncertainty of the corrected results may be challenging to determine.	Calibration can be done with a finite-duration force that has a known time profile, or with a force step or pulse that is sufficiently rapid to be treated as instantaneous.

peaks in the balance dynamic response. This again maximizes available digitizer dynamic range, often improving signal-to-noise ratio, which is of high importance in interpreting the dynamic data. The hardware filter becomes a part of the balance dynamic response. These uses of hardware filtering are in addition to the anti-aliasing function that must be implemented with such filters.

1. *Use of Reduced-Order Models*

Detailed finite element models are time-consuming to construct and can be computationally expensive to solve when using a large number of degrees of freedom. Smaller-degree-of-freedom models, referred to as reduced-order models, have the ability to approximately estimate the first few natural frequencies of a system and predict the dynamic response in an efficient manner.

Additionally, reduced-order models can provide key information to the practitioner as safety and measurement quality decisions are made in the design phase of wind tunnel test structures. Identifying the location of the first resonant mode and the source of the mode can provide insight into the likelihood of exciting this mode and whether the excitation of this mode may prevent accurate dynamic measurements. It can also add insight into test system design changes that can be made to increase the resonant frequencies. Changes to test article mass as well as the balance and sting stiffnesses are effectively captured by the reduced-order model.

Here, we present a reduced-order model, which may be representative of a wind tunnel test setup that can be used to estimate the dynamics of the system. For this math model, we assume the following:

1) There are predominantly two degrees of freedom wherein the flexible elements are the balance and the sting.

2) The test article is much stiffer than the balance and can be treated as a rigid mass.

3) The sting is supported by a rigid structure.

The schematic shown in Fig. 4 is representative of a test configuration that is dominated by translational motion; however, other test configurations may be better represented using rotational motions. A slender sting can be modeled as a beam, and its displacement can

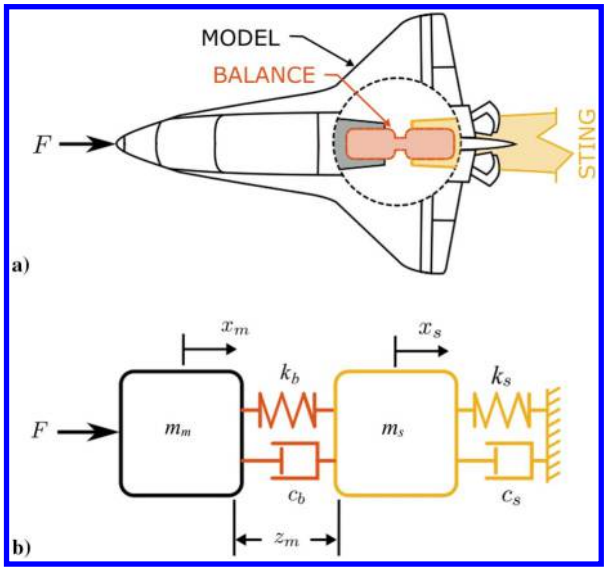

Fig. 4 a) Schematic of a wind tunnel test article mounted onto a balance and a nonrigid sting. b) An equivalent reduced-order dynamic model of the system.

be represented by either a translation or a rotation. In practice, there will be a combination of rotational and translational motion, and motions occur in three-dimensional space, consisting of six degrees of freedom (three rotations and three translations). Under the assumption that the motions in different planes are not coupled, these models can be used to approximate the dynamics in one plane, then the parameters can be changed to approximate the dynamics in another plane.

2. *Translational Dominant Motions*

In practice, the sting is a distributed parameter structure and, consequentially, has many natural frequencies. Here, the sting is

modeled with an equivalent reduced-order stiffness k_s and mass m_s, which approximately describe the beam dynamics up to and slightly beyond the first natural frequency. The values of m_s and k_s depend on the geometry of the sting and can be tabulated from their properties as given in reference texts such as Ref. [23]. The test article is assumed to be a rigid lumped mass, while the balance is considered to be the flexible element with stiffness k_b. The sting and the balance are assumed to have damping, denoted by c_s and c_b, respectively, which is proportional to the velocity. Unlike the mass and stiffness quantities, damping is not easily determined and is dependent upon a number of factors, including geometry and material choices. However, the damping coefficients do not affect the estimation of the natural frequencies of the system. The governing equations of motion for the structure shown in Fig. 4 are given to be

$$m_m\ddot{x}_m + c_b(\dot{x}_m - \dot{x}_s) + k_b(x_m - x_s) = F \tag{1}$$

$$m_s\ddot{x}_s + k_s x_s + c_s\dot{x}_s + c_b(\dot{x}_s - \dot{x}_m) + k_b(x_s - x_m) = 0 \tag{2}$$

where x_m is the total axial displacement of the test article, and x_s is the axial displacement of the sting. The balance will output an indicator (typically a voltage) that is proportional to the deflection of the balance or the relative motion between the test article and the sting, defined as $z_m = x_m - x_s$. Upon substituting this relation into Eqs. (1) and (2), the governing equations of motion become

$$m_m(\ddot{z}_m + \ddot{x}_s) + c_b\dot{z}_m + k_b z_m = F \tag{3}$$

$$m_s\ddot{x}_s + k_s x_s + c_s\dot{x}_s - c_b\dot{z}_m - k_b z_m = 0 \tag{4}$$

For design purposes, it is useful to examine the frequency response functions of Eqs. (3) and (4). Letting $\mathcal{L}$ denote the Laplace transform and $\mathcal{L}\{x(t)\} = X(s)$, where s is the complex frequency, Eqs. (3) and (4) can be written in terms of transfer functions. The frequency response functions are found by making the substitution $s \mapsto j\omega$, where $j = \sqrt{-1}$, resulting in

$$\frac{Z_m(\omega)}{F(\omega)} = \frac{-\omega^2 m_s + j\omega c_s + k_s}{(-\omega^2 m_m + j\omega c_b + k_b)(-\omega^2 m_s + j\omega c_s + k_s) - \omega^2 m_m(j\omega c_b + k_b)} \tag{5}$$

$$\frac{Z_s(\omega)}{F(\omega)} = \frac{j\omega c_m + k_m}{(-\omega^2 m_m + j\omega c_b + k_b)(-\omega^2 m_s + j\omega c_s + k_s) - \omega^2 m_m(j\omega c_b + k_b)} \tag{6}$$

The quantity Z_m in Eq. (5) is proportional to the signal output from the balance for a given applied force F. The amplitude response is taken to be the absolute value of Eq. (5), $|Z_m/F|$, while the phase is the angle between the real and imaginary parts of Z_m/F. Similarly, the amplitude response of the sting is given by the absolute value of Eq. (6), $|Z_s/F|$, and the phase is the angle between the real and imaginary parts of Z_s/F. Often, it is instructive to express frequency response functions using nondimensional parameters. The following nondimensional parameters are defined:

$$\omega_m = \sqrt{k_s/m_s}, \qquad \omega_s = \sqrt{k_s/m_s}, \qquad \zeta_m = \frac{c_m}{2m_m\omega_m},$$
$$\zeta_s = \frac{c_s}{2m_s\omega_s}, \qquad \eta = \frac{m_m}{m_s}$$

The quantity ω_m is the uncoupled natural frequency of the balance and test article, while ω_s is the uncoupled natural frequency of the sting. The quantities ζ_m and ζ_s are the damping ratios of the uncoupled test article-balance and sting, respectively. The effective mass ratio is given to be η. Equations (5) and (6) can then be written as

$$\frac{Z_m(\omega)}{F(\omega)} = \frac{\frac{1}{k_b}\left[1 - \left(\frac{\omega}{\omega_s}\right)^2 + j2\zeta_s\left(\frac{\omega}{\omega_s}\right)\right]}{\left[1 - \left(\frac{\omega}{\omega_m}\right)^2 + j2\zeta_m\left(\frac{\omega}{\omega_m}\right)\right]\left[1 - \left(\frac{\omega}{\omega_s}\right)^2 + j2\zeta_s\left(\frac{\omega}{\omega_s}\right)\right] - \eta\left(\frac{\omega}{\omega_s}\right)^2\left[1 - j2\zeta_m\left(\frac{\omega}{\omega_m}\right)\right]} \tag{7}$$

$$\frac{Z_s(\omega)}{F(\omega)} = \frac{\frac{1}{k_s}\left[j2\zeta_m\left(\frac{\omega}{\omega_m}\right) + 1\right]}{\left[1 - \left(\frac{\omega}{\omega_m}\right)^2 + j2\zeta_m\left(\frac{\omega}{\omega_m}\right)\right]\left[1 - \left(\frac{\omega}{\omega_s}\right)^2 + j2\zeta_s\left(\frac{\omega}{\omega_s}\right)\right] - \eta\left(\frac{\omega}{\omega_s}\right)^2\left[1 - j2\zeta_m\left(\frac{\omega}{\omega_m}\right)\right]} \tag{8}$$

While the equations in this section have been derived for a balance and sting subject to axial load, they are also valid for bending motions (in the normal and side planes) as demonstrated in the next section.

3. *Example Case Study*

Figure 5 shows a test configuration of a rocket that was tested in a low-speed wind tunnel. A translational two-degree-of-freedom model has been assembled to model the systems behavior based on the parameters listed in Table 2. This model assumes that the balance and the sting are the flexible elements in the system with displacements driven by translational degrees of freedom. Furthermore, the test article can be treated as a rigid mass, and the sting is supported by a rigid structure. The inputs for this model were assembled from computer aided design files of the test configuration, which produced mass estimates based on volume and density information from the

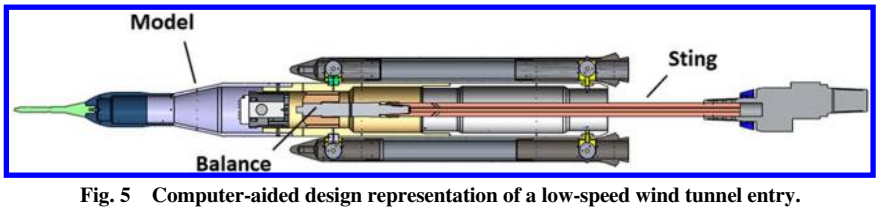

Fig. 5 Computer-aided design representation of a low-speed wind tunnel entry.

Table 2 Summary of the inputs into the two-degree-of-freedom model

Mass of test article, m_m	140 kg
Mass of sting/balance assembly, m_s	12 kg
Stiffness of balance, k_b	1 MN/m
Stiffness of sting, k_s	60 kN/m
Dampening of balance, c_b	200 kg/s
Dampening of sting, c_s	20 kg/s

test article. Stiffness inputs were estimated using finite element techniques as illustrated in Fig. 6. Here, a load was applied to the end of the sting that mates with the balance (of sufficient magnitude that deflection would be reasonable without exceeding the yield strength of the material) and fixed boundary conditions were applied to the other end of the sting. The global deflection of the sting was then used to estimate the stiffness based on an applied force to measured displacement ratio (100 N/1.68 mm = 60 kN/m). A similar process was carried out for the balance applying a known load to the metric end and applying fixed constraints to the nonmetric end. Handbook calculations can also be used to approximate the stiffness. Analytical calculations typically exist for many common sting geometries.

The response of the system based on the two-degree-of-freedom model [Eqs. (7) and (8)] is shown in Fig. 7a. Note that Eqs. (7) and (8) have been multiplied by k_b and k_s, respectively, which is common practice in the dynamics community to make the response dimensionless. The first resonant mode is driven by the sting and occurs at 3 Hz. The second mode is an antiresonant mode experienced by the balance at 11 Hz. The balance output is proportional to Z_m; therefore, if loads approaching 3 Hz and above are being measured as part of this test campaign, the static calibration may no longer be suitable to maintain accuracy requirements for the test. The balance senses more load than is actually being imparted to the system due to the first mode. Therefore, dynamic loads measured at 3 Hz or greater using the static calibration sensitivity will be overestimates of the true loads. But for the antiresonant mode at 11 Hz, the balance senses less load than is being applied to the test article. Therefore, dynamic loads measured at approximately 11 Hz using the static calibration sensitivity will be underestimates of the true loads. For the damping coefficients assumed for this model, the static calibration only appears to be valid for measurements below about 1 Hz. Trying to measure faster events using the static calibration will introduce measurement uncertainty as evidenced by the departure of $k_b * Z_m/F$ from unity above 1 Hz. From a data acquisition standpoint, this means that simply increasing the sampling rate will not allow faster force events to be captured accurately because the wind tunnel system is effectively acting like a mechanical filter accentuating or attenuating the balance sensitivity depending on the frequency.

Figure 7b illustrates the effect of system response on the balance when the stiffness parameters listed in Table 2 are individually varied by an order of magnitude while leaving all other parameters constant. Increasing the stiffness of the balance by an order of magnitude to $k_b = 10$ MN/m results in a modest change of the first natural frequency to 3.6 Hz (from 3 Hz using nominal parameters) but a large change in the second natural frequency at 168 Hz (from 49 Hz using nominal parameters). For this structure, increasing the stiffness

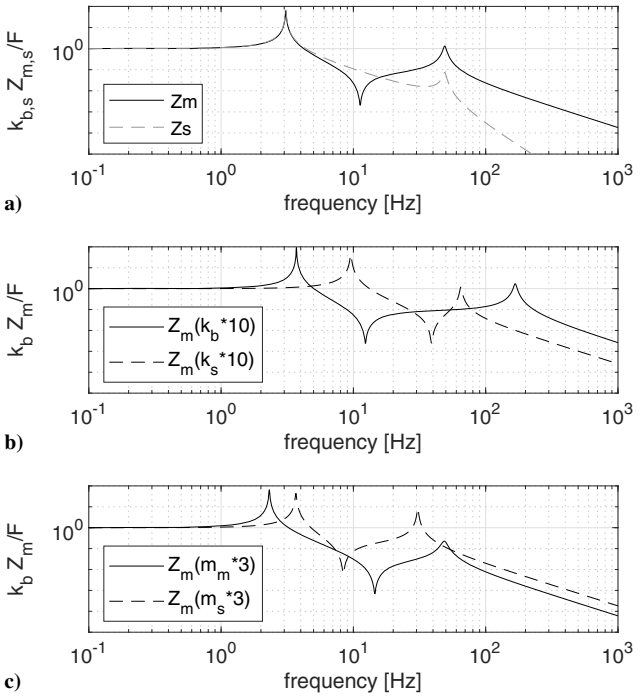

Fig. 7 Response of system based on a) nominal parameters defined in Table 2, b) order of magnitude increases of the sting and balance stiffnesses, and c) factor of three increases of the sting and test article masses.

of the sting to $k_b = 0.6$ MN/m more than doubles the first natural frequency to 9.6 Hz, while the second natural frequency moves up to approximately 65 Hz.

The effect of increasing the mass of the test article or sting is shown in Fig. 7c. When the mass of the test article is increased by a factor of three, the first resonance decreases to 2.3 Hz, while the second remains largely the same at approximately 49 Hz. On the other hand, when increasing the mass of the sting by a factor of three, the first natural frequency increases slightly to 3.7 Hz, while the second natural frequency decreases to 31 Hz.

B. Measurement of the Dynamic Response

While estimates of the wind tunnel test configuration dynamic response via reduced-order models or simulations provide insightful design information, a more complete understanding of the dynamic response of the system can be determined through experimental characterization of the system. It is best to complete characterization of the system in its fully assembled state in the wind tunnel to estimate parameters such as dampening coefficients, which can be altered by slight modifications to the test setup.

The dynamic response of a system is usually measured using one of three approaches:

1) *Cut wire:* Using this approach, a calibrated mass is hung from the test system with a thin wire. The wire is then severed, allowing the mass to fall freely due to gravity while applying a step load to the test system. There are numerous examples of this approach being used for wind tunnel test systems [11,24,25].

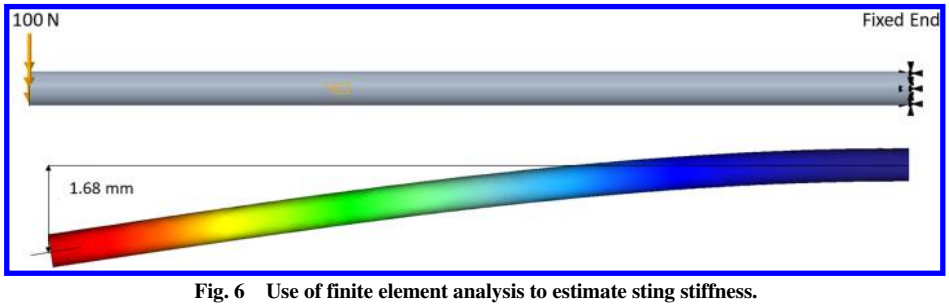

Fig. 6 Use of finite element analysis to estimate sting stiffness.

2) *Impact hammer:* An impact hammer can also be used to apply a dynamic force. An impact hammer has only small variations from user to user, making it well suited as a transfer standard [1]. Impact hammers have been used to evaluate wind tunnel test systems [15,24].

3) *Shaker:* A shaker can also be used to produce forces over a large frequency range. A shaker has been used to develop a model that captures the dynamic behavior of a wind tunnel balance [26]. A downside of the shaker is that it is unlikely to be installed in situ in the wind tunnel facility, which can introduce errors as the system is transferred from the shaker to the wind tunnel.

A successful dynamic characterization will depend on the objectives of the test and could range from completing a modal survey to identify regions to avoid during testing based on test safety considerations to completing a dynamic force calibration as discussed in the next section. These objectives will guide the type and placement of instrumentation on the system as well as the locations for dynamic excitation. These technical considerations are beyond the scope of this work, but the reader is referred to Ref. [18] for specific guidance.

To provide some context for what can be learned from measuring the dynamic response of a wind tunnel test system, a dynamic verification was performed to a rotorcraft test stand by applying a swept-sinusoidal force using a shaker with a force transducer mounted onto the end of the shaker. In principle, because the force was applied using a calibrated transducer, the data could be used in a dynamic calibration as well. The force was swept over 180 s in the frequency range of 5–20 Hz. In practice, it is desirable to apply the force over a lower frequency range of interest, but the frequency range was limited by the response of the shaker. The output signals of the force transducer and the force balance were simultaneously recorded. The Fourier transforms of the two signals were divided and are shown in Fig. 8. It is noted that, in this frequency range, the response closely resembles that of the two-degree-of-freedom response shown in the previous section, although there are other dynamic features in the 7.25–8 Hz regime. For this specific structure, the first resonance occurs around 6.1 Hz, which would erroneously amplify forces near this frequency. In contrast, forces with frequency content near the antiresonance around 9.2 Hz would be attenuated. The information in this graph can be used to estimate the dynamic error for a given bandwidth or signal profile as was done in the earlier example.

C. Dynamic Compensation Strategies

If it is not possible to avoid making balance measurements that are affected by the system dynamics, a number of approaches can be taken to compensate for the dynamic distortion. We describe two approaches here, one being the use of acceleration measurements to compensate for inertial forces, and the other being the use of dynamic calibration to interpret the balance output signal. These are two of the most prominent dynamic compensation approaches; however, a variety of other approaches do exist.

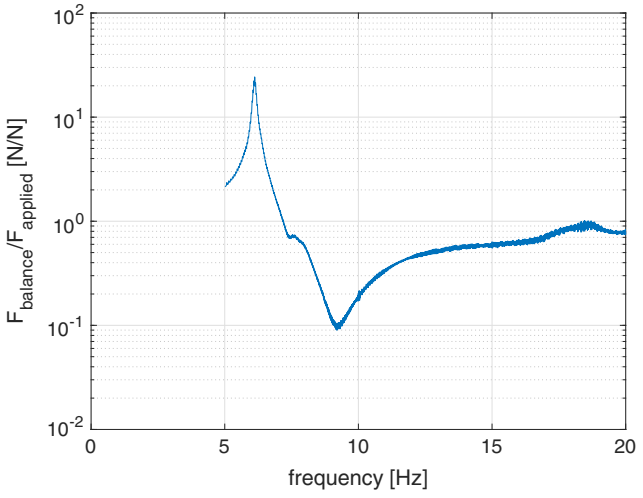

Fig. 8 Frequency response of a balance mounted in a rotorcraft test stand relative to the applied force.

1. *Acceleration Compensation*

The dynamic distortions are predominantly due to the inertia (Ma) of accelerated masses (e.g., the test article), which are interposed between the balance flexure and the force of interest. These inertial terms can be added to the force sensed by the balance in order to give a significantly more accurate measurement of the force applied to the test article. Acceleration compensation has been used by numerous researchers to make dynamic wind tunnel force measurements [8,9,17,21,27–29]. For an example of this technique, consider a uniaxial force measurement performed on the system shown in Fig. 5, with the reduced-order model shown in Fig. 4. As discussed in Sec. III.A [Eq. (3)], the deformation of the balance $z_m(t)$ is related to the applied force $F(t)$ by

$$m_m\ddot{x}_m + c_b\dot{z}_m + k_b z_m = F \tag{9}$$

Note that z_m is the relative displacement between the two ends of the balance (in a inertial frame), while x_m is the absolute position of the balance in the inertial frame (see Fig. 4 for further clarity). The force indicated by the balance based on its static sensitivity is $F_{\text{balance}}(t) = k_b z_m(t)$. Thus, the ratio $F_{\text{balance}}(t)/F(t)$ is

$$\frac{F_{\text{balance}}}{F} = \frac{k_b z_m}{F} = \left(1 + \frac{m_m\ddot{x}_m + c_b\dot{z}_m}{k_b z_m}\right)^{-1} \tag{10}$$

whereas for a perfectly accurate measurement this ratio would be 1.

Attaching an accelerometer to the lumped mass m_m consisting of the test article and part of the balance allows the inertia of this lumped mass to be added to $F_{\text{balance}}(t)$ to yield $F_{\text{corr}}(t)$:

$$F_{\text{corr}}(t) = F_{\text{ind}}(t) + ma_m(t) = k_b z_m(t) + m_m\ddot{x}_m(t) \tag{11}$$

The ratio $F_{\text{corr}}(t)/F(t)$ is then

$$\frac{F_{\text{corr}}}{F} = \left(1 + \frac{c_b\dot{z}_m}{k_b z_m + m_m\ddot{x}_m}\right)^{-1} \tag{12}$$

To the extent that the reduced-order model is an accurate representation of the test assembly, the dynamic errors are greatly reduced and the remaining uncorrected error is due to damping forces. In practice, there will also be errors in the accelerometer measurements due to accelerometer calibration error, cross-coupling of acceleration vector components, and noise. In most real tests, we may expect that the errors in approximating the assembly by a reduced-order model consisting of a few lumped masses will dominate at higher frequencies (e.g., close to and above the first resonant frequency).

Using the procedure presented in Sec. III.A to go from the time domain to the frequency domain, we obtain the frequency response functions $F_{\text{balance}}(\omega)/F(\omega)$ and $F_{\text{corr}}(\omega)/F(\omega)$. Using the parameter values given in Table 2, we plot the magnitudes of these in Fig. 9a, illustrating the reduction in dynamic error due to the acceleration compensation. We show results for both a perfectly accurate acceleration measurement (F_{corr}), and an acceleration measurement with a 2% error at all frequencies ($F_{\text{corr,measured}}$). Uncertainty in the few-percent range can be achieved in dynamic acceleration measurements with calibrated commercial accelerometers under favorable measurement conditions. Other sources of error, such as the balance measurements and simplifying the distributed test assembly as a reduced-order model, are not included given the focus on acceleration compensation. We see that the acceleration compensation results in greatly improved force measurements, indicated by the ratios $F_{\text{corr}}(\omega)/F(\omega)$ and $F_{\text{corr,measured}}(\omega)/F(\omega)$ being close to unity except in the vicinity of resonances. Dynamic distortion at frequencies around resonances remains. Above the first resonance frequency at 3 Hz, the force is dominated by inertia; in other words, in this

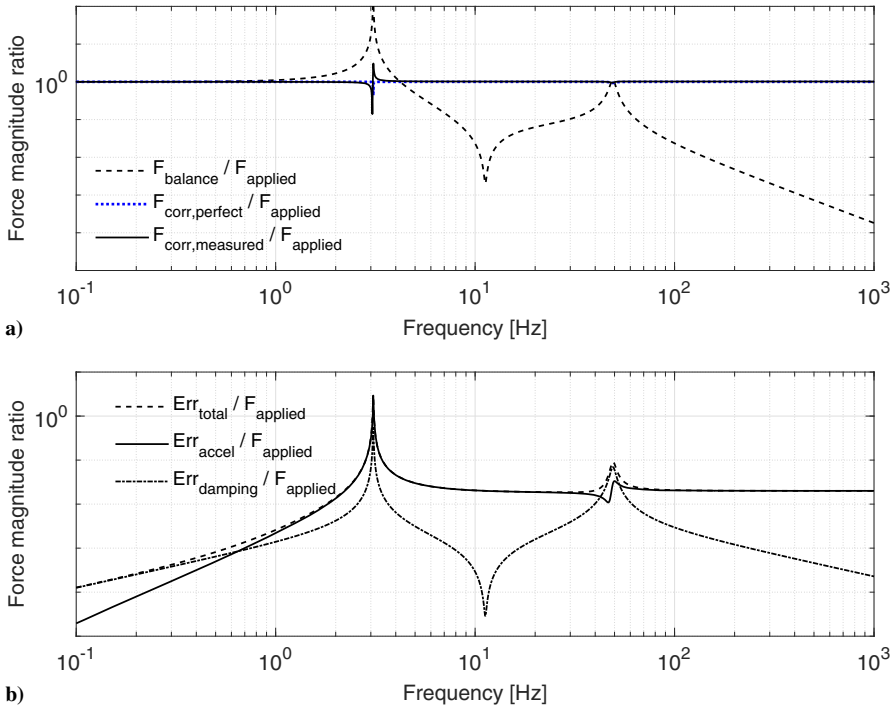

Fig. 9 a) Lines showing ratios of indicated force to applied force with and without acceleration compensation. b) Contribution of errors due to neglected damping term and assumed 2% acceleration measurement error.

frequency range the (corrected) force measurement is given essentially by the accelerometer, the balance contribution being small.

In Fig. 9b, we show the errors in $F_{\text{corr,measured}}(\omega)/F(\omega)$ due to the assumed 2% acceleration measurement error, and due to damping. We see that the accelerometer error is larger than the error due to dissipation over most of the frequency range where the correction is significant. At the 3 Hz resonance, the 2% acceleration error corresponds to an error in the compensated force of ≈300%, and the error due to damping is also significant (≈60% in this case). In practice, the approximation inherent in the reduced-order model will lead to additional error that grows with frequency and in general becomes significant as the first resonance frequency is approached. Using finite-element models can allow an increased accuracy of acceleration compensation, although the problem becomes increasingly difficult if the test article has resonances within the measurement bandwidth of interest [30,31]. Within the reduced-order paradigm, the structure of the test article and balance may necessitate using a larger number of lumped elements than the two considered here, to get adequate representation over the frequency range of interest, thus requiring additional acceleration measurements. The number of directions in which the acceleration must be measured also increases with the number of force and moment components in the test having dynamic behavior. Last, although it was discussed briefly, uncertainty associated with dynamic measurements is currently a major focus in the metrological community with growing interest for specific dynamic measurement applications [41–45]. As measurements continue to push to higher 6 bandwidths, accurate uncertainty evaluations will become increasingly important in the metrological community as well as for dynamic aerospace measurement applications.

2. *Dynamic Calibration*

A conceptually more straightforward approach is to calibrate the system dynamically, by methods such as those listed above in Sec. III.B, and then use the obtained dynamic sensitivity to interpret the force transducer output. In other words, one uses a known force $F_{\text{cal}}(\omega)$ in the calibration to determine the sensitivity $S(\omega) \equiv V_{\text{cal}}(\omega)/F_{\text{cal}}(\omega)$, and then one determines the force $F(\omega)$ in the test as $F(\omega) = V(\omega)/S(\omega)$. The force as a function of time $F(t)$ is obtained from $F(\omega)$ by an inverse Fourier transform. The procedure can also be carried out entirely in the time domain, but the operations cannot be represented in the time domain as simple products and ratios of functions.

This approach is not reliant on a reduced-order model, includes damping force contributions, and can compensate resonances; it also does not require supplementary acceleration measurements. It is important to note that the response of the balance is dependent upon the location of the applied force, which poses additional challenges. For instance, often the integrated force acting on the test article is the desired measured quantity of interest; however, most calibration techniques apply a force at a localized point, such as the instrumented hammer and cut wire methods. The applicable distributed elastic response of the test article may differ from the point load response, introducing some error. Additionally, forces applied at a point may also induce moments onto the test article, which need to be considered in the calibration. Moreover, if the test article is flexible and has resonant frequencies within the frequency range of interest, the data analysis presented within this section becomes considerably more difficult [30,31].

These advantages come at the cost of the dynamic calibration and potentially an increased complexity of data analysis. Mathematically implementing this with available methods, such as the frequency-domain method that will be used below, does rely on the assumption that the system is linear and time invariant. Small deviations from this are generally present for real systems, and they may contribute meaningfully to uncertainty of the measurement. There are many examples of this approach being applied to dynamic wind tunnel force measurements, especially for hypersonic impulse tests, for example [24,25,32–35].

We illustrate dynamic compensation based on dynamic calibration using the two-degree-of-freedom test assembly with parameters given in Table 2, for which the frequency response function of the balance is shown in Fig. 7a (test article response z_m). The equivalent time domain impulse response function of the balance is shown in Fig. 10 and is given by the inverse Fourier transform of the frequency response function. This impulse response function represents the response of the system to an infinitely narrow applied force pulse, and it is the shape of the response observed in practice for a real pulse that is much narrower than the fastest significant dynamics of the system. The impulse response function provides the response of the system to a real finite-duration force input $F(t)$ by the convolution theorem [36,37]

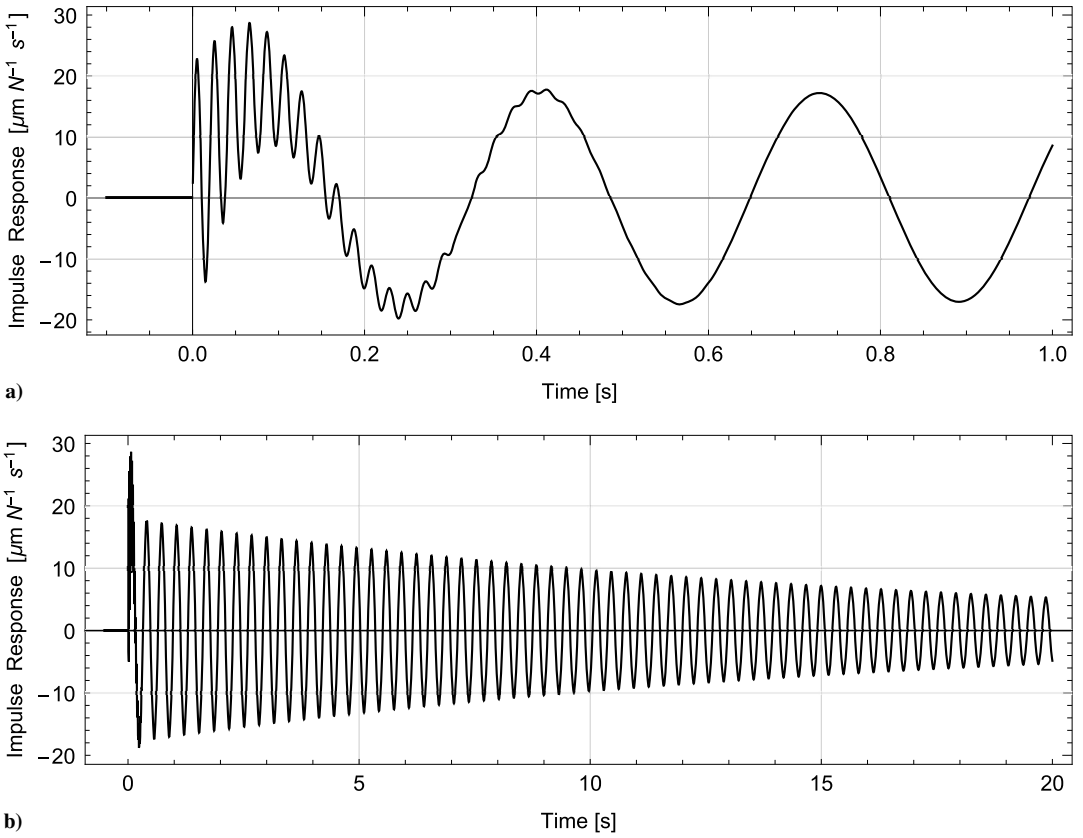

Fig. 10 Balance impulse response function obtained from reduced-order model of test assembly shown on two different timescales.

$$z_m(t) = \int_{-\infty}^{\infty} F(\tau)h(t-\tau)\,\mathrm{d}\tau \tag{13}$$

where $h(t)$ is the impulse response function of the balance. We observe in Fig. 10 an initial time window in which the 49 Hz balance resonance dominates the response, which transitions to the 3 Hz sting resonant response at longer times, decaying away after approximately 100 s. If a constant wind tunnel load were suddenly applied to the assembly for a static test, this is the time duration it would take for the oscillatory response to decay away and leave only the static response.

The response of the system to a Gaussian-shaped force pulse $F(t) = F_{\mathrm{p}}e^{-(1/2)((t-t_0)/w)^2}$ is considered, where F_{p} is the peak height of the pulse and w characterizes the pulse width. The response is obtained using the convolution Eq. (13). As expected and as indicated by Eq (13), this balance output $z_m(t)$ depends on both the applied force pulse $F(t)$ and the balance dynamics (captured by the impulse response function $h(t)$); sufficiently short force pulses will result in the higher frequency resonant behavior being observable, while longer force pulses will not excite this mode. We consider two force pulses of peak force 250 N, shown in Fig. 11a, with half-maximum full widths of 10 and 100 ms, respectively. Figure 11b shows the initial portion of the system response to these two pulses. The narrower pulse excites both the 49 Hz resonance and the 3 Hz resonance, with the 49 Hz resonance decaying away after approximately 0.5 s. The wider pulse excites only the 3 Hz resonance, because the applied force pulse does not contain enough frequency content at 49 Hz to excite the resonance at that frequency. The

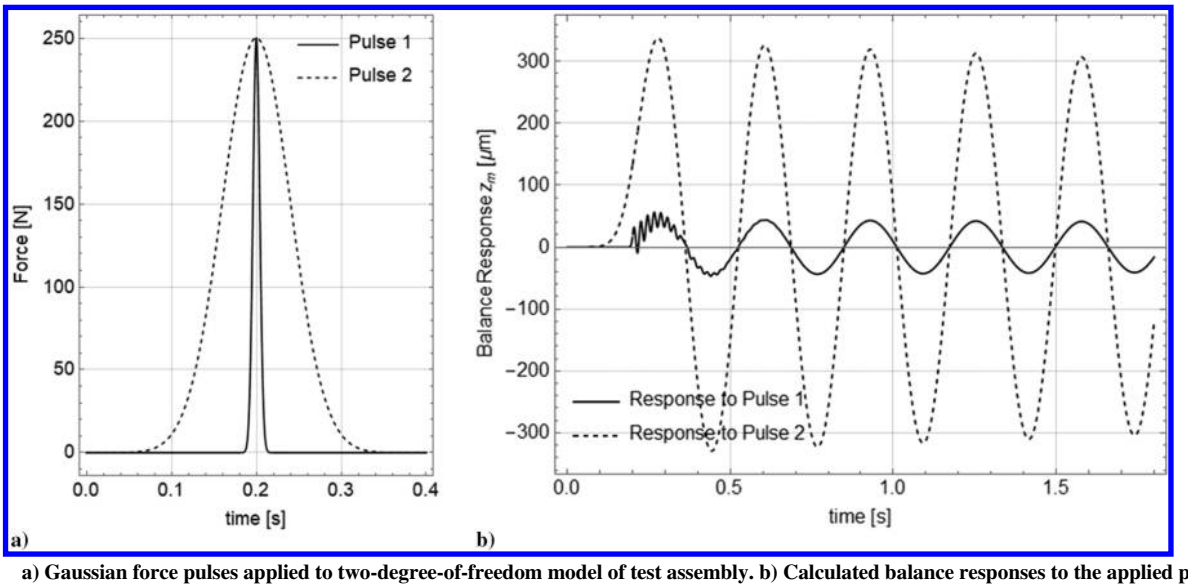

Fig. 11 a) Gaussian force pulses applied to two-degree-of-freedom model of test assembly. b) Calculated balance responses to the applied pulses.

magnitude of the two responses is proportional to the integrals of the respective applied force pulses, and as such, the magnitude of the wider pulse is 10 times larger than the narrow one. In both cases, the 3 Hz resonant response decays away after approximately 100 s, as expected from the impulse response function.

To compensate for the dynamic response of the balance, the dynamic response must be determined by some type of dynamic calibration, which is generally a nontrivial task. We consider that this has been done to high accuracy, with only a small amount of error. For this example, we take the impulse response function shown in Fig. 10 as the true impulse response function of the balance. We assume that this has been measured with an overall scaling error of 0.5% and an added white noise of RMS amplitude 0.05% times the peak amplitude of the impulse response; that is, we modify the true impulse response function shown in Fig. 10 by including these errors, to model the calibrated impulse response function to use in compensating the balance output. Compensating the balance output using the dynamic calibration means deconvolving the (imperfectly) calibrated impulse response from the balance output [24,37]. We perform this deconvolution in the frequency domain, according to the following sequence of operations.

1) Assuming that we start with a digitally sampled sequence of balance output $F_{\text{balance}}[\text{n}]$, and the calibrated impulse response function $h[\text{n}]$ sampled at the same uniformly spaced sequence of time instants $\text{n}\Delta t$, we transform both to the frequency domain:

$$F_{\text{balance}}[\text{m}] = \text{DFT}\{F_{\text{balance}}[\text{n}]\} \tag{14}$$

$$H[\text{m}] = \text{DFT}\{h[\text{n}]\} \tag{15}$$

where DFT indicates the discrete Fourier transform. The frequency spacing of the discrete frequency samples m is $1/T$, where T is the

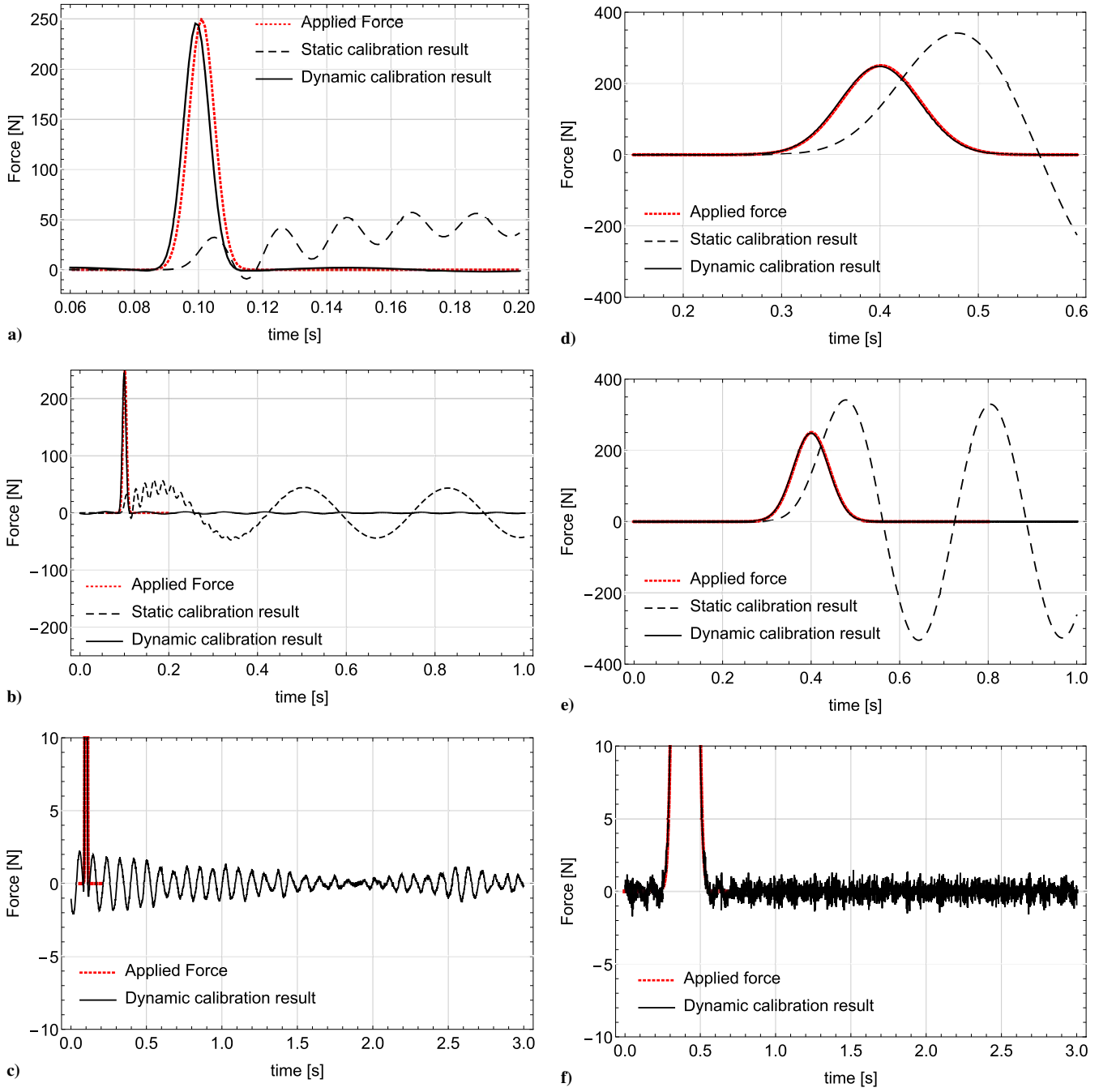

Fig. 12 Balance force indications based on static and dynamic calibrations for a Gaussian pulse with a–c) 10 ms half-width and d–f) 100 ms half-width. The figures show the results with different horizontal and vertical scales.

total duration of the time series, and it is assumed that both time traces are of the same length and collected with the same sampling interval Δt. We take Δt to be 1 ms in the present example and use time traces of 100 s duration (100,000 samples), resulting in a spacing of the frequency samples of 0.01 Hz. Furthermore, we simulate measurement noise by adding white noise, of RMS amplitude $\approx 10^{-5}$ times the peak output signal, to the acquired force samples $F_{\text{balance}}[\text{n}]$.

2) The estimated applied force F_{est} in the frequency domain at each frequency point is then

$$F_{\text{est}}[\text{m}] = F_{\text{balance}}[\text{m}]R[\text{m}]/H[\text{m}] \tag{16}$$

where we have introduced the regularization filter $R[\text{m}]$. This is used to stabilize the compensation, which is a so-called "inverse operation," by suppressing regions of the data where the signal-to-noise ratio is low, and it is up to the metrologist to choose. This choice can be based, for example, on an expectation of the signal-to-noise level as a function of frequency, given the input signal and the calibrated balance frequency response function. Discussion of optimizing the choice of regularization filter is, however, beyond the scope of this article, and it is the subject of monographs such as Refs. [38,39]. Without the regularization, regions of low signal-to-noise ratio corrupt the time-domain estimate obtained in the next step, often greatly. However, the regularization filter attenuates true signal content as well as noise. In the present example, we use a third-order Butterworth low-pass filter with a cutoff frequency of 200 Hz. In some cases, the data may be of sufficiently high quality to get an acceptable result without the introduction of $R[\text{m}]$.

3) The inverse discrete Fourier transform is used to obtain the input force in the time domain:

$$F_{\text{est}}[\text{n}] = \text{IDFT}\{F_{\text{est}}[\text{m}]\} \tag{17}$$

corresponding to estimated force values at the time instants $\text{n}\Delta t$.

Some prerequisite signal processing knowledge is required to avoid errors and pitfalls in performing procedure described above. Detailed discussion is beyond the scope of this paper, and we refer the reader to texts such as Ref. [40].

In Fig. 12, we show the estimated applied force resulting from such dynamic compensation of the balance output, for the two pulses in Fig. 11a. We also show the force that would be inferred based on a static calibration, which is completely erroneous. For consistency, we have included the same 0.5% scaling error in the static calibration as in the dynamic calibration, although the effect of this is too small to be visible on the plotted static-calibration-based result. The dynamic compensation recovers the applied pulse shape quite accurately, although an erroneous roughly 12 Hz component of small amplitude is evident ($\approx$0.5% of the peak force amplitude for the narrower force pulse and $\approx$0.2% for the wider force pulse). This 12 Hz component can be understood due to the antiresonance in the frequency response at that frequency, meaning that the signal-to-noise ratio at that frequency is low, and our choice of regularization filter as a 200 Hz bandwidth low-pass filter did not suppress this region. In the case of the narrower pulse, a regularization filter that did suppress the region around 12 Hz would corrupt the measurement significantly, as the narrow pulse has significant spectral content up to approximately 80 Hz.

IV. Conclusions

This paper has presented an introduction to dynamic force measurement concepts emphasizing wind tunnel testing applications. Different techniques of varying complexity have been presented to introduce the reader to the available techniques that have been used to make accurate dynamic measurements. An example reduced-order model has been shown that can serve as a design and predictive tool to estimate the bandwidth wherein the static sensitivity may be used to make measurements with acceptable errors. An acceleration compensation technique was discussed that can be used in conjunction with a model to apply inertial corrections to the measured force. Moreover, a dynamic calibration method was presented that can be used to estimate the applied forces over a relatively large bandwidth at the cost of more complex signal processing methods.

The methods and examples discussed within this paper have been constructed in one direction corresponding to one component of load in order to simplify the analysis and dynamic response concepts. For a higher-fidelity representation, six directions corresponding to the six components of load (three forces and three moments) must be considered resulting in lumped-parameter models with more than two degrees of freedom. For example, a reduced-order model of a test article and sting, where both the test article and sting are treated as rigid lumped masses connected by springs and dampers, would require 12 degrees of freedom if considering all six components of load. These additional degrees of freedom, while not always necessary depending on test objectives, contribute to dynamic measurement uncertainty and can increase the complexity of acceleration compensation and dynamic calibration.

Acknowledgments

Thanks to Austin Overmeyer (DEVCOM AvMC) for providing realistic wind tunnel model data. Devin Burns and Peter Parker were supported by the NASA Aerosciences Evaluation and Test Capabilities (AETC) Project.

References

[1] Vlajic, N., and Chijioke, A., "Traceable Calibration and Demonstration of a Portable Dynamic Force Transfer Standard," *Metrologia*, Vol. 54, No. 4, 2017, pp. S83–S98. https://doi.org/10.1088/1681-7575/aa75da

[2] Kumme, R., "Dynamic Investigations of Force Transducers," *Experimental Techniques*, Vol. 17, No. 6, 1993, pp. 13–18. https://doi.org/10.1111/j.1747-1567.1993.tb00784.x

[3] Schlegel, C., Kieckenap, G., Glöckner, B., Buß, A., and Kumme, R., "Traceable Periodic Force Calibration," *Metrologia*, Vol. 49, No. 3, 2012, pp. 224–235. https://doi.org/10.1088/0026-1394/49/3/224

[4] Balakrishna, S., Butler, D., Acheson, M., and White, E., "Design and Performance of an Active Sting Damper for the NASA Common Research Model," *49th AIAA Aerospace Sciences Meeting Including the New Horizons Forum and Aerospace Exposition*, AIAA Paper 2011-0953, 2011. https://doi.org/10.2514/6.2011-953

[5] Burt, G. E., and Uselton, J. C., "Effect of Sting Oscillations on the Measurement of Dynamic Stability Derivatives," *Journal of Aircraft*, Vol. 13, No. 3, 1976, pp. 210–216. https://doi.org/10.2514/3.58650

[6] Glaese, R., Bales, G., Hsu, S., Mor, M., and Stirling, B., "Reduction of Dynamic Response of a Wind Tunnel Sting Mount Using a Hub Damper Unit," *48th AIAA Aerospace Sciences Meeting Including the New Horizons Forum and Aerospace Exposition*, AIAA Paper 2010-1307, 2010. https://doi.org/10.2514/6.2010-1307

[7] Bernstein, L., "Force Measurements in Short-Duration Hypersonic Facilities," Advisory Group for Aerospace Research and Development North Atlantic Treaty Organization, AGARDograph No. 214, 1975, https://apps.dtic.mil/sti/citations/ADA018842.

[8] Ledford, R. L., Smotherman, W. E., and Kidd, C. T., "Recent Developments in Heat-Transfer-Rate, Pressure, and Force Measurements for Hot-Shot Tunnels," *IEEE Transactions on Aerospace and Electronic Systems*, Vol. AES-4, No. 2, 1968, pp. 202–209. https://doi.org/10.1109/TAES.1968.5408959

[9] Duryea, G. R., and Martin, J. F., "An Improved Piezoelectric Balance for Aerodynamic Force," *IEEE Transactions on Aerospace and Electronic Systems*, Vol. AES-4, No. 3, 1968, pp. 351–359. https://doi.org/10.1109/TAES.1968.5408988

[10] Simmons, J., "Measurement Techniques in High-Enthalpy Hypersonic Facilities," *Experimental Thermal and Fluid Science*, Vol. 10, No. 4, 1995, pp. 454–469. https://doi.org/10.1016/0894-1777(94)00066-H

[11] Sahoo, N. K., and Reddy, K. P. J., "Force Measurement Techniques for Hypersonic Flows in Shock Tunnels," *International Journal of Hypersonics*, Vol. 1, No. 1, 2010, pp. 31–58. https://doi.org/10.1260/1759-3107.1.1.31

[12] Ballmann, J., Boucke, A., Chen, B., Reimer, L., Reimer, L., Behr, M., Behr, M., Dafnis, A., Buxel, C., Buesing, S., Buesing, S., Reimerdes, H., Reimerdes, H., Kordt, M., Kordt, M., Brink-Spalink, J., Brink-Spalink, J., Theurich, F., Buscher, A., and Buscher, A., "Aero-Structural Wind Tunnel Experiments with Elastic Wing Models at High Reynolds Numbers (HIRENASD—ASDMAD)," *49th AIAA Aerospace Sciences Meeting including the New Horizons Forum and Aerospace Exposition*, AIAA Paper 2011-0882, 2012.
https://doi.org/10.2514/6.2011-882

[13] Ritter, M., Neumann, J., and Krüger, W. R., "Aeroelastic Simulations of High Reynolds Number Aero Structural Dynamics Wind Tunnel Model," *AIAA Journal*, Vol. 54, No. 6, 2016, pp. 1962–1973.
https://doi.org/10.2514/1.J053384

[14] Wieseman, C. D., Chwalowski, P., Heeg, J., Boucke, A., and Castro, J., "Structural Dynamics Modeling of HIRENASD in support of the Aeroelastic Prediction Workshop," *54th AIAA/ASME/ASCE/AHS/ASC Structures, Structural Dynamics, and Materials Conference*, AIAA Paper 2013-1801, 2013.
https://doi.org/10.2514/6.2013-1801

[15] Britt, R., Ortega, D., Tigue, J. M., and Scott, M., "Wind Tunnel Test of a Very Flexible Aircraft Wing," *53rd AIAA/ASME/ASCE/AHS/ASC Structures, Structural Dynamics and Materials Conference*, AIAA Paper 2012-1464, 2012.
https://doi.org/10.2514/6.2012-1464

[16] Waite, J., Bartels, R. E., and Stanford, B., "Aeroelastic Model Development for the Integrated Adaptive Wing Technology Maturation Project Wind-Tunnel Test," *AIAA Aviation 2020 Forum*, AIAA Paper 2020-2717, 2020.
https://doi.org/10.2514/6.2020-2717

[17] Beaussier, J., "A Six-Component Balance," *IEEE Transactions on Aerospace and Electronic Systems*, Vol. AES-4, No. 2, 1968, pp. 210–217.
https://doi.org/10.1109/TAES.1968.5408960

[18] Ewins, D. J., *Modal Testing: Theory, Practice and Application*, Wiley, Hoboken, NJ, 2009, Chap. 1.

[19] Meirovitch, L., *Fundamentals of Vibrations*, Waveland Press, Long Grove, IL, 2010, Chap. 12.

[20] Jessen, C., and Grönig, H., "A New Principle for a Short-Duration Six Component Balance," *Experiments in Fluids*, Vol. 8, No. 3, 1989, pp. 231–233.
https://doi.org/10.1007/BF00195800

[21] Storkmann, V., Olivier, H., and Gronig, H., "Force Measurements in Hypersonic Impulse Facilities," *AIAA Journal*, Vol. 36, No. 3, 1998, pp. 342–348.
https://doi.org/10.2514/2.402

[22] Kazemba, C., Braun, R., Clark, I., and Schoenenberger, M., "Survey of Blunt Body Dynamic Stability in Supersonic Flow," *AIAA Atmospheric Flight Mechanics Conference*, AIAA Paper 2012-4509, 2012.
https://doi.org/10.2514/6.2012-4509

[23] Young, W. C., and Budynas, R. G., *Roark's Formulas for Stress and Strain*, Vol. 7, McGraw–Hill, New York, 2002, Chap. 8.

[24] Mee, D. J., "Dynamic Calibration of Force Balances for Impulse Hypersonic Facilities," *Shock Waves*, Vol. 12, No. 6, 2003, pp. 443–455.
https://doi.org/10.1007/s00193-003-0181-6

[25] Sanderson, S. R., and Simmons, J. M., "Drag Balance for Hypervelocity Impulse Facilities," *AIAA Journal*, Vol. 29, No. 12, 1991, pp. 2185–2191.
https://doi.org/10.2514/3.10858

[26] Gorbushin, A., and Bolshakova, A., "Unsteady Axial Force Measurement by the Strain Gauge Balance," *Measurement*, Vol. 152, Feb. 2020, Paper 107381.
https://doi.org/10.1016/j.measurement.2019.107381

[27] Marineau, E. C., "Force Measurements in Hypervelocity Flows with an Acceleration Compensated Piezoelectric Balance," *Journal of Spacecraft and Rockets*, Vol. 48, No. 4, 2011, pp. 697–700.
https://doi.org/10.2514/1.A32047

[28] Draper, J. W., Lee, S., and Marineau, E. C., "Development and Implementation of a Hybrid Dynamic Force Measurement System at AEDC Tunnel 9," *58th AIAA/ASCE/AHS/ASC Structures, Structural Dynamics, and Materials Conference*, AIAA Paper 2017-1593, 2017.
https://doi.org/10.2514/6.2017-1593

[29] Holden, M., "Experimental Studies of the Effects of Asymmetric Transition on the Aerothermal Characteristics of Hypersonic Blunted Slender Cones," *23rd Aerospace Sciences Meeting*, ACS Paper 1985-325, 1985.
https://doi.org/10.2514/6.1985-325

[30] Lage, Y. E., Maia, N. M. M., and Neves, M. M., "Force Magnitude Reconstruction Using the Force Transmissibility Concept," *Shock and Vibration*, Vol. 2014, April 2014, Paper 905912.
https://doi.org/10.1155/2014/905912

[31] Logan, P., Avitabile, P., and Dodson, J., "Reconstruction of External Forces Beyond Measured Points Using a Modal Filtering Decomposition Approach," *Experimental Techniques*, Vol. 44, No. 1, 2020, pp. 113–125.
https://doi.org/10.1007/s40799-019-00340-0

[32] Mee, D. J., Daniel, W. J. T., and Simmons, J. M., "Three-Component Force Balance for Flows of Millisecond Duration," *AIAA Journal*, Vol. 34, No. 3, 1996, pp. 590–595.
https://doi.org/10.2514/3.13108

[33] Abdel-jawad, M. M., Mee, D. J., and Morgan, R. G., "New Calibration Technique for Multiple-Component Stress Wave Force Balances," *Review of Scientific Instruments*, Vol. 78, No. 6, 2007, Paper 065101.
https://doi.org/10.1063/1.2744235

[34] Draper, J. W., and Lee, S., "Development of Hypersonic Wind Tunnel Force Measurement Using Deconvolution of Acceleration Data," *AIAA Scitech 2019 Forum*, AIAA Paper 2019-0940, 2019.
https://doi.org/10.2514/6.2019-0940

[35] Ngo, C., Powell, J., and Ross, J. C., "Inverse Force Determination on a Small Scale Launch Vehicle Model Using a Dynamic Balance," *55th AIAA Aerospace Sciences Meeting*, AIAA Paper 2017-1405, 2017.
https://doi.org/10.2514/6.2017-1405

[36] Cheever, E., "The Convolution Integral," 2020, https://lpsa.swarthmore.edu/Convolution/Convolution.html [retrieved 24 Jan. 2021].

[37] Riad, S. M., "The Deconvolution Problem: An Overview," *Proceedings of the IEEE*, Vol. 74, No. 1, 1986, pp. 82–85.
https://doi.org/10.1109/PROC.1986.13407

[38] Vogel, C. R., *Computational Methods for Inverse Problems*, SIAM, Philadelphia, 2002, Chap. 3.
https://doi.org/10.1137/1.9780898717570

[39] Hansen, P. C., *Discrete Inverse Problems: Insight and Algorithms*, SIAM, Philadelphia, 2010, Chap. 4.
https://doi.org/10.1137/1.9780898718836

[40] Oppenheim, A. V., and Schafer, R. W., *Discrete-Time Signal Processing*, 3rd ed., Pearson, Upper Saddle River, NJ, 2010, Chap. 4.

[41] Eichstädt, S., Wilkens, V., Dienstfrey, A., Hale, P., Hughes, B., and Jarvis, C., "On Challenges in the Uncertainty Evaluation for Time-Dependent Measurements," *Metrologia*, Vol. 53, No. 4, 2016, Paper S125.
https://doi.org/10.1088/0026-1394/53/4/S125

[42] Eichstädt, S., and Wilkens, V., "Evaluation of Uncertainty for Regularized Deconvolution: A Case Study in Hydrophone Measurements," *Journal of the Acoustical Society of America*, Vol. 141, No. 6, 2017, pp. 4155–4167.
https://doi.org/10.1121/1.4983827

[43] Elster, C., Link, A., and Bruns, T., "Analysis of Dynamic Measurements and Determination of Time-Dependent Measurement Uncertainty Using a Second-Order Model," *Measurement Science and Technology*, Vol. 18, No. 12, 2007, p. 3682.
https://doi.org/10.1088/0957-0233/18/12/002

[44] Elster, C., and Link, A., "Uncertainty Evaluation for Dynamic Measurements Modelled by a Linear Time-Invariant System," *Metrologia*, Vol. 45, No. 4, 2008, p. 464.
https://doi.org/10.1088/0026-1394/45/4/013

[45] Hale, P. D., Dienstfrey, A., Wang, J. C., Williams, D. F., Lewandowski, A., Keenan, D. A., and Clement, T. S., "Traceable Waveform Calibration with a Covariance-Based Uncertainty Analysis," *IEEE Transactions on Instrumentation and Measurement*, Vol. 58, No. 10, 2009, pp. 3554–3568.
https://doi.org/10.1109/TIM.2009.2018012